APPLIED PHYSICS

Making flexible spin caloritronic devices with interconnected nanowire networks

Tristan da Câmara Santa Clara Gomes, Flavio Abreu Araujo, Luc Piraux*

Spin caloritronics has recently emerged from the combination of spintronics and thermoelectricity. Here, we show that flexible, macroscopic spin caloritronic devices based on large-area interconnected magnetic nanowire networks can be used to enable controlled Peltier cooling of macroscopic electronic components with an external magnetic field. We experimentally demonstrate that three-dimensional CoNi/Cu multilayered nanowire networks exhibit an extremely high, magnetically modulated thermoelectric power factor up to 7.5 mW/K^{2}m and large spin-dependent Seebeck and Peltier coefficients of −11.5 μV/K and −3.45 mV at room temperature, respectively. Our investigation reveals the possibility of performing efficient magnetic control of heat flux for thermal management of electronic devices and constitutes a simple and cost-effective pathway for fabrication of large-scale flexible and shapeable thermoelectric coolers exploiting the spin degree of freedom.

INTRODUCTION

The ability of thermoelectric materials to harvest waste heat and deliver cooling power through solid-state devices without moving parts makes them important candidates of sustainable energy technologies in the future. Innovative spin-based transport mechanisms are crucial steps in developing the next generation of thermoelectric materials (*1*). In this context, coupling heat-driven transport with spintronics is at the heart of the rapidly emerging field of spin caloritronics (*2*, *3*). Previous studies on nanoscale precision magnetic structures such as lithographically defined nanopillars have led to the observation of various spin-enabled mechanisms such as spin Seebeck effects (*4*, *5*), thermally driven spin injection (*6*), and thermally assisted spin-transfer torque (*7*, *8*). However, key issues to observe the magnetic control of heat flux in a spintronic device are related to insufficient power generation capability and difficulties in detecting extremely small temperature changes in such nanostructures. Although there have been some initial studies on the thermoelectric analogs of giant magnetoresistance (GMR) in magnetic multilayers with current in-plane configuration (*9*–*12*), the effects of interfaces make the interpretation of the results more delicate than in the simpler CPP (current-perpendicular-to-plane) configuration (*13*). In the limit of no-spin relaxation, most of the CPP-GMR data can be understood using a simple two-current series resistor model, in which the resistance of layers and interfaces simply adds and where "up" and "down" charge carriers are propagating independently in two spin channels with large spin asymmetries of the electron's scattering (*14*, *15*).

Similarly, the spin-dependent thermoelectric effects exploit the fact that the Seebeck coefficients for spin-up and spin-down electrons, $S_\uparrow$ and $S_\downarrow$, are also different because of the exchange splitting of the d-band (*16*, *17*). The 3d ferromagnetic metals exhibit relatively large diffusion thermopowers because of the pronounced structure of the d-band and the high energy derivative of the density of states at the Fermi level. Besides, these magnetic metals also exhibit substantial magnon-drag contribution to the thermoelectric power within a wide temperature range (*18*, *19*). Moreover, the largest room temperature (RT) power factor (PF = $S^2\sigma$, with σ as the electrical conductivity), which is the physical parameter that relates to the output power density of a thermoelectric material, is achieved for cobalt (PF ≈ 15 mW/K^{2}m) (*20*).

To date, most of the investigations of thermoelectric transport in CPP-GMR systems were performed on lithographically defined nanopillars, single nanowire (NW), and parallel NW arrays (*21*–*24*). The thermoelectric properties of nanostructures are more challenging to measure than in bulk materials since it is difficult to determine and/or eliminate contact thermal resistance, an important error source, and simulations are often required to estimate the temperature gradient over the multilayer stacks (*6*, *23*, *25*, *26*). Therefore, accurate determination of the spin-dependent Seebeck coefficients still remains challenging, and from these previous works, only relatively small RT values of $S_\uparrow - S_\downarrow$ ranging from −1.8 to −4.5 μV/K for cobalt and permalloy, respectively, were indirectly estimated from measurements performed on nanopillar devices (*6*, *27*). In addition, observations of net Peltier cooling in these magnetic nanostructures have not been possible because of the dominant Joule heating effect compared to the Peltier effect together with the technical issues in detecting extremely small temperature changes. Besides, the thermoelectric PFs of CPP-GMR nanopillar and NW systems were not determined from these experiments. Spin-dependent Seebeck and Peltier effects were also recently reported in magnetic tunnel junctions (*25*, *26*, *28*). Although magnetic tunnel junctions are expected to be suitable materials for magnetic switching by virtue of thermal spin-torque (*8*), the high electrical resistance (in the kilohm range) and the nanometer junction size prevent their use for thermoelectric Peltier coolers due to the dominant Joule heating effect. A recent experimental study made on magnetic tunnel junctions leads to change in temperature due to the magneto-Peltier effect of the order of ~100 μK at RT for an electric current density of several kiloamperes per square centimeter (*28*). So, despite the practical significance, all these experimental issues impose strong restrictions on applications in the burgeoning field of spin caloritronics.

In this study, we developed an experimental platform that allows for the observation of magnetically controlled heat flux in custom-fabricated spin caloritronic devices. Specifically, we fabricated macroscopic interconnected networks made of CoNi/Cu NWs by direct electrodeposition into three-dimensional (3D) nanoporous polymer host membranes (see Materials and Methods) (*29*, *30*). This fabrication strategy allows us to move from submicrometer-scale magnetic nanostructures to more efficient macroscopic-scale spin caloritronics

Institute of Condensed Matter and Nanosciences, Université catholique de Louvain, Place Croix du Sud 1 bte L7.04.02, 1348 Louvain-la-Neuve, Belgium.
*Corresponding author. Email: luc.piraux@uclouvain.be

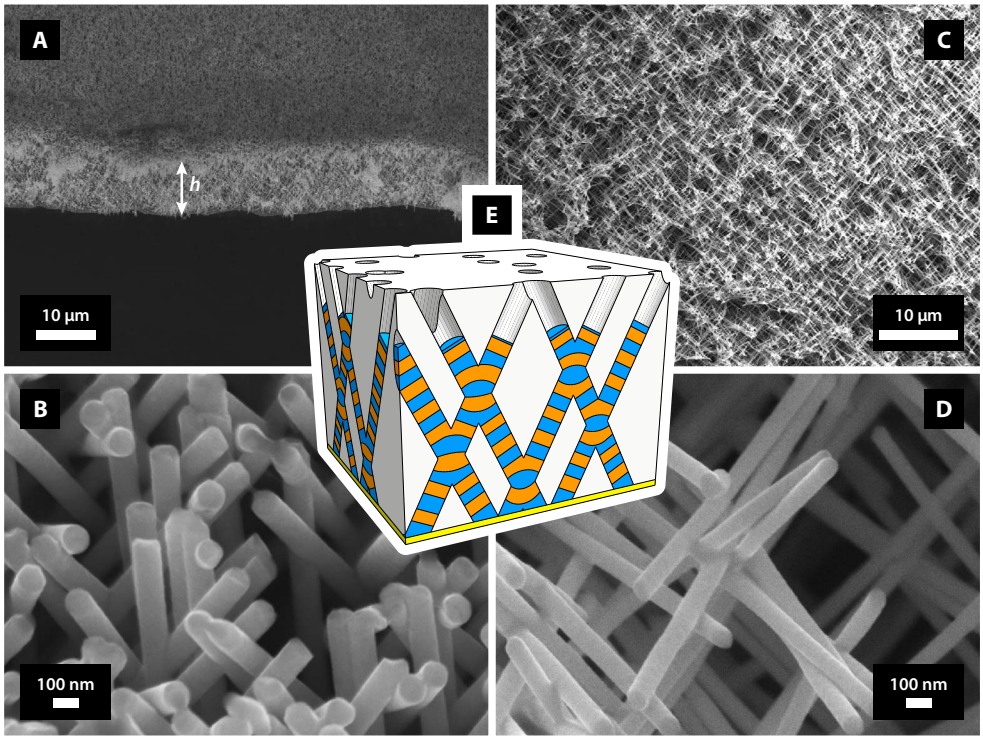

Fig. 1. 3D interconnected NW networks. (**A** to **D**) Scanning electron microscopy (SEM) images of self-supported interconnected nanowire (NW) networks with different magnifications, diameters, and packing densities. Low-magnification image showing the 50° tilted view of the macroscopic NW network film with 105-nm diameter and 22% packing density (A) and SEM image at higher magnification showing the NW branched structure (B). Low-magnification image showing the top view of the NW network with 80-nm diameter and 3% packing density (C) and SEM image at higher magnification (D) corresponding to (C). (**E**) Schematic of the interconnected NW network with alternating magnetic and nonmagnetic layers embedded within the 3D nanoporous PC template.

devices. Besides, electrical connectivity is essential to allow charge flow over the whole sample sizes. The multilayered NW network films based on the CPP geometry combine numerous advantages, such as the high thermoelectric PF and large magnetothermoelectric effects that can be easily determined using simple but precise measurement setups. Using centimeter-scale NW network films, we demonstrated net Peltier cooling of macroscopic electronic components and efficient control of the heat flow using a magnetic field. Also, our experimental measurements enable reliable determination of key spin-dependent material parameters over a wide temperature range. Another significant advantage of our approach is the achievement of highly efficient flexible and shapeable spin caloritronics devices. Moreover, since there is no sample size limitation, the fabrication method is directly expandable into NW network films with much larger dimensions.

RESULTS

The interconnected nanoporous templates have been prepared by performing a sequential two-step exposure to energetic heavy ions, at angles of +25° and −25°, with respect to the normal of the polycarbonate (PC) membrane surface (for details, see Materials and Methods) (*31*). Two different 22-μm-thick polymer membranes were used in this study with diameters of 80 and 105 nm and very different porosity characteristics. The spin caloritronic devices are networks of interconnected NWs embedded inside the 3D polymer membranes.

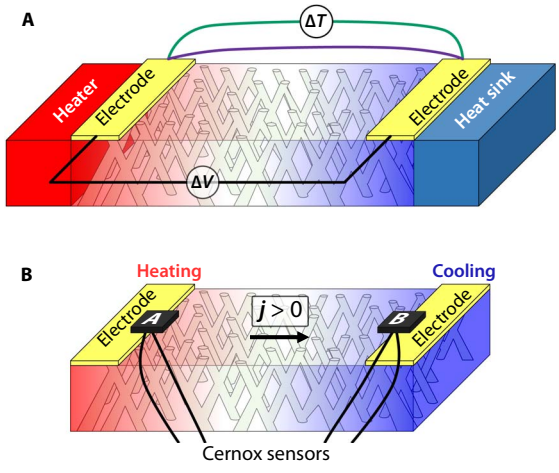

Fig. 2. Experimental setups for spin caloritronic measurements. (**A**) Device configuration to measure the Seebeck coefficient and the magnetothermoelectric effect. Heat flow is generated by a resistive element, and a thermoelectric voltage ΔV is created by the temperature difference ΔT between the two metallic electrodes that is measured by a thermocouple (see Materials and Methods for details). (**B**) Device architecture and measurement configuration for the Peltier cooling/heating detection. Two Cernox temperature sensors A and B are used to probe the local temperature change at the electrode—NW network junctions induced by the electric current flow (see Materials and Methods for details). Device dimensions in (A) and (B) are 15 mm long, 5 mm wide, and 22 μm thick, and the color represents the generated temperature profile in the NW networks. The gold electrodes are 2 mm wide.

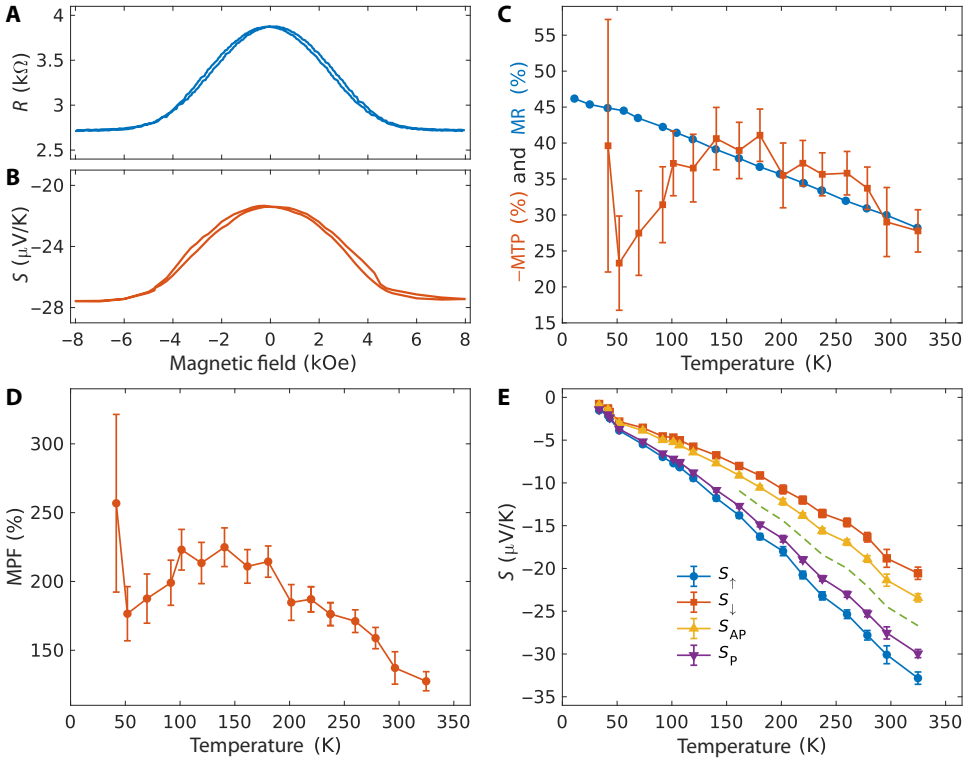

Fig. 3. Measured thermoelectric characteristics. (**A** and **B**) Electrical resistance (A) and Seebeck coefficient (B) of a CoNi/Cu NW network showing similar magnetic field dependence corresponding to MR = 30.2% and MTP = −29.3% at RT. The magnetic field was applied in the plane of the NW network film. (**C**) MR ratio and −MTP as a function of temperature. (**D**) MPF as a function of temperature obtained using the MR and MTP data in (C) and MPF = $(1 - MTP)^2/(1 - MR) - 1$. (**E**) Measured Seebeck coefficients at zero applied field S_{AP} (orange triangles) and at saturating magnetic field S_P (violet triangles), along with the corresponding calculated $S_\uparrow$ (blue circles) and $S_\downarrow$ (red squares) from Eqs. 1 and 2 (see text). The dashed green line represents the Seebeck coefficient for a vanishing MR effect. Data in the whole figure have been acquired using the same interconnected network made of NWs with a diameter of 80 nm and a packing density of 3%. The error bars in (C) to (E) reflect the uncertainty of the voltage and temperature measurements as described in section S6.

The crossed NWs with a multilayer structure of CoNi/Cu were grown in the host porous templates by pulsed electrochemical deposition (*32*). The thickness of the bilayers was set as 15 nm with approximately the same thickness for the CoNi and Cu layers. Figure 1 (A to D) displays the morphology of self-supported interconnected NW samples obtained after template dissolution, whereas Fig. 1E illustrates the 3D multilayered architecture. As schematically outlined in Fig. 2, we developed two experimental setups allowing to simultaneous measure the magnetoresistance and Seebeck coefficient (Fig. 2A) and to determine the Peltier heating and cooling power generated at the electrodes of the flexible NW network films (Fig. 2B) (see Materials and Methods).

Spin-dependent thermoelectric transport in CoNi/Cu NW networks

As shown in Fig. 3 (A and B), the resistance and thermopower of the low-packing density CoNi/Cu NW sample show the same magnetic field dependencies and relative changes of ~30% at $H = 8$ kOe at RT. The absolute value of the magnetothermopower MTP = $(S_{AP} - S_P)/S_{AP}$, with S_{AP} and S_P as the corresponding thermopowers in the high- and low-resistance states, respectively, shows a similar increase with decreasing temperature as the MR ratio (defined as MR = $(R_{AP} - R_P)/R_{AP}$) for temperatures larger than 130 K (see Fig. 3C). However, below this temperature, the MTP exhibits a less pronounced effect and reaches a minimum value around −25% at $T = 50$ K, where a further increase at lower temperatures results in MTP values up to about −40%.

The Seebeck coefficients at RT are measured to be −21.3 μV/K in the AP state and −27.6 μV/K in the P state, and the MTP reaches about 30%. These values are in agreement with the results obtained from measurements carried out on a single CoNi/Cu NW (*24*). Calculations of the thermoelectric PF at RT lead to $PF_{AP} = S_{AP}^2/\rho_{AP} \approx 3.1$ mW/K^{2}m and $PF_P = S_P^2/\rho_P \approx 7.5$ mW/K^{2}m (see section S2 for the estimation of the resistivity values), which are comparable values or even larger than the PF of the widely used thermoelectric material, bismuth telluride (in the range of 1 to 5 mW/K^{2}m) (*33*). Besides, the PF values obtained for CoNi/Cu NW networks embedded in polymer membranes are at least one order of magnitude larger than those of flexible thermoelectric films based on optimized conducting polymers (*34*). The magneto-PF (MPF = $(PF_P - PF_{AP})/PF_{AP}$) reaches ~135% at RT and exceeds 200% at low temperatures, as also shown in Fig. 3D. The efficiency of a material's thermoelectric energy conversion is determined by its figure of merit $ZT = S^2\sigma T/\kappa$, with κ the thermal conductivity. Because of the very low thermal conductivity of PC (κ = 0.2 W/m K at RT), the contribution of the polymer matrix to heat transport is much smaller than that of the metallic NW network. For metallic NWs, heat transport is dominated by the electron heat conduction flux (*35*), so assuming that the Wiedemann-Franz law holds, an estimate of the electronic thermal conductivity at RT gives κ_E = 50 W/m K in the AP configuration and κ_E = 72 W/m K in the P configuration. In this case, the figure of merit is reduced to $ZT = S^2/L_0$, with L_0 the Lorenz number. Using this approximation, we obtain

$ZT = 3.1 \times 10^{-2}$ at RT at magnetically saturated state for the CoNi/Cu NW sample. Although the RT *ZT* value in this CoNi/Cu CNW sample is about one order of magnitude smaller than that in BiTe alloys, it is comparable to those of thermocouple alloys ($ZT = 6 \times 10^{-2}$ and $ZT = 1.4 \times 10^{-2}$ in constantan and chromel, respectively) and can be used in applications for devices with low energy requirements when the supply of heat essentially is free as with waste heat. Moreover, recent work (*36*) suggests that traditionally used high-ZT thermoelectric materials are not the more appropriate materials for electronic cooling applications. In case the goal is to cool hot spots, the Peltier current is in the same direction as the natural conduction heat flux, and materials with larger PFs and large thermal conductivities should be used. In this context, magnetic multilayered NW networks are good candidates for active cooling (*36*).

Using the parameter $\beta = (\rho_\downarrow - \rho_\uparrow)/(\rho_\downarrow + \rho_\uparrow)$ characterizing the asymmetry in the resistivity between the two spin conduction channels in ferromagnetic layers, the spin-dependent Seebeck coefficients $S_\uparrow$ and $S_\downarrow$ can be expressed as follows (see section S3)

$$S_\uparrow = \frac{1}{2}\left[S_{AP}(1-\beta^{-1}) + S_P(1+\beta^{-1})\right] \quad (1)$$

$$S_\downarrow = \frac{1}{2}\left[S_{AP}(1+\beta^{-1}) + S_P(1-\beta^{-1})\right] \quad (2)$$

The temperature evolutions of S_{AP}, S_P, $S_\uparrow$, and $S_\downarrow$ are shown in Fig. 3E. Although magnon-drag may contribute to the thermopower for some temperature range, the Seebeck effect in the NW networks is dominated by the diffusion contribution as indicated by the nearly linear decrease of the Seebeck coefficients with decreasing temperature and the relationship between thermoelectric power and resistivity reported in section S4. The estimated values at RT are $S_\uparrow = -30.2\ \mu V/K$, $S_\downarrow = -18.7\ \mu V/K$, and $S_\uparrow - S_\downarrow = -11.5\ \mu V/K$ using $\beta = (MR^{1/2}) = 0.55$, which are similar to those previously reported in bulk Co ($S_\uparrow = -30\ \mu V/K$ and $S_\downarrow = -12\ \mu V/K$) (*17*). From Eqs. 1 and 2, it can be easily deduced that $S_\uparrow = S_P$ and $S_\downarrow = S_{AP}$ in the limit of an extremely large MR ratio ($\beta \to 1$). Since the MTP can also be expressed as $MTP = 2\beta\eta/(1+\beta\eta)$, where $\eta = (S_\downarrow - S_\uparrow)/(S_\downarrow + S_\uparrow)$ denotes the spin asymmetry for Seebeck coefficients (see section S3), infinitely large MTP and MPF effects are expected when the product $\beta\eta$ tends to −1. In previous works performed using both Ni and ferromagnetic dilute alloys with the occurrence of a virtual bound state at the Fermi level (*16*, *17*), $S_\uparrow$ and $S_\downarrow$ were found to have an opposite

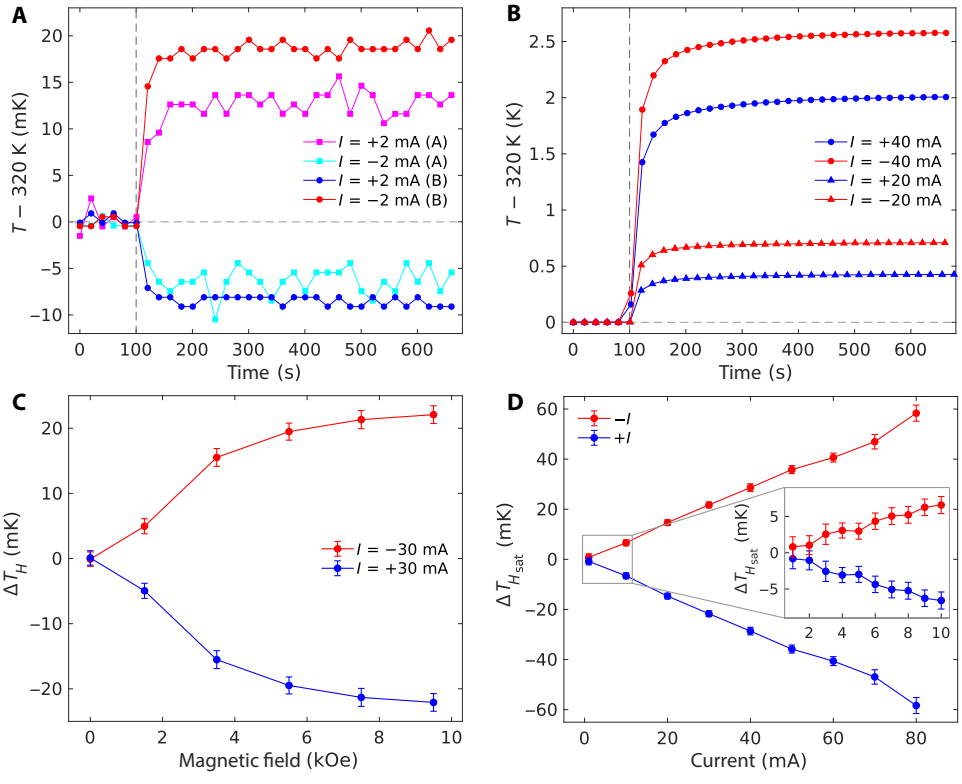

Fig. 4. Direct observation of Peltier, Joule, current crowding, and magneto-Peltier effects. (**A**) Temperature versus time traces of the sum of the Joule and Peltier heats relative to a working temperature of 320 K, as recorded by the Cernox sensors A and B (see Fig. 2B). A direct current of 2 mA is applied both forward and reverse in the interconnected CoNi/Cu NWs that are 105 nm in diameter and with a packing density of 22% (R = 1.8 ohms, MR = 6.3%). (**B**) Same as in (A) but for higher current intensities for which the Peltier effect becomes dominated by the Joule heating, i.e., I = 20 and 40 mA, and restricted to data recorded at sensor B. Both in (A) and (B), the DC current is switched on after 100 s as shown by the vertical dashed lines. (**C**) Measured temperature changes ΔT_H at the Peltier junction B during the magnetic field sweep for DC currents of −30 and +30 mA. Here, the contribution from the Peltier heating has been estimated (section S5). The Peltier term leads to heating and cooling at the saturation field of 9.5 kOe and depends on current flow direction. (**D**) Measured total temperature changes $\Delta T_{H_{sat}}$ at the Peltier junction B between the zero-field (T_{H_0}) and saturated states ($T_{H_{sat}}$) versus current intensity applied both forward and reverse. Inset: Data obtained in the low-current range. The error bars in (C) and (D) reflect the uncertainty of the temperature measurements as described in section S6.

sign, which corresponds to $|\eta| > 1$. Therefore, the fabrication of multilayered NWs with appropriate magnetic layer composition should make it possible to fine-tune the PF of thermoelectric energy conversion with an external magnetic field.

Magnetic control of Peltier cooling

Current flow in the high-packing density CoNi/Cu NW sample results in Joule heating and a Peltier heat current at the junctions between the NW network and the gold electrodes. These heat flows were monitored continuously from the temperature changes using Cernox sensors (A and B, as shown in Fig. 2B) with respect to the operating temperature T = 320 K for different current intensities and polarities, as well as for various applied magnetic fields. Net cooling occurs at low currents when the direction of the Peltier heat current flow is such that $\Pi I < 0$ at the considered junction (with Π as the Peltier coefficient) and dominates over the Joule heating effect (RI^2), as shown in Fig. 4A. When the DC current flows from the NWs (with the higher Peltier coefficient) to the gold electrode (with the lower one), the Peltier heat is released from the junction, i.e., net cooling happens for I = +2 mA at sensor B, while net heating happens at sensor A (see Fig. 4A). As expected, the situation is reversed when the current flows in the opposite direction. For currents larger than 5 mA, the Joule heating dominates over the Peltier cooling, as shown by two representative temperature versus time traces for I = ±20 and ±40 mA (see Fig. 4B). Unlike the Peltier effect that leads to a cooling or a heating of the system depending on the direction of current flow, the Joule effect does not depend on the current polarity. It is thus possible to separate the two effects linearly (see section S5). From Fig. 4B, one can estimate the Peltier cooling ability of the NW network of ~7.5 K/A.

As shown in Fig. 4C, the magneto-Peltier effect has been quantified by recording the temperature change ΔT_H during the magnetic field sweeps. The field dependence of ΔT_H resembles that of MR. The same measurements were performed for different currents, as shown in Fig. 4D, where the total temperature change ($\Delta T_{H_{sat}} = T_{H_0} - T_{H_{sat}}$) between the zero-field (T_{H_0}) and saturation ($T_{H_{sat}}$) states is reported. As expected, the magneto-Peltier effect increases linearly with the driving current. From these results, one can obtain the guideline for the magnitude of the magnetically controlled cooling and heating ability of a macroscopic electronic component against the injected current. Using the values of $S_\uparrow$ and $S_\downarrow$ from Fig. 3E and the Onsager relation, which relates the two thermoelectric coefficients $\Pi = ST$, one may estimate the maximum difference between the Peltier coefficients in the AP and P states for an infinite MR ratio as $\Pi_\uparrow - \Pi_\downarrow$, which correspond to −3.45 mV at RT for CoNi/Cu NWs. Since currents up to a few hundreds of milliamperes are able to pass through the densely packed NW films without damaging the network structure, we may anticipate that a magnetic field can switch a heat flow as large as 1 mW.

DISCUSSION

We have experimentally demonstrated magnetic field control of the Peltier cooling of electronic components using efficient and macroscopic-scale spin caloritronic devices built from CoNi/Cu NW networks. We have found very high thermoelectric PF up to 7.5 mW/K^{2}m at RT, which are larger values than the PF of the widely used thermoelectric material, bismuth telluride. The PF is magnetically modulated with a PF change ratio greater than 150%. Moreover, key spin-dependent material parameters were extracted accurately over a wide temperature range. Large spin-dependent Seebeck and Peltier coefficients of −11.5 and −3.45 mV were obtained at RT, respectively.

This work should stimulate further systematic exploration and optimized growth of a variety of 3D NW networks with high magnetothermoelectric performance. We anticipate that the use of less-resistive NW network films with larger packing factor and thickness up to 100 μm should significantly enhance the ability of net refrigerating effect controlled by a magnetic field. The dimensions of such 3D NW networks are highly scalable, and we can anticipate that they might be used as shapeable thermoelectric components for hot-spot cooling of electronic devices. In principle, realization of planar NW-based thermoelectric modules as small as ~1 mm^2 can be made. Such dimensions are appropriate to fit a variety of practical applications requiring effective temperature management of sensors and integrated circuits. In addition, a practical thermoelectric cooler made of flexible and lightweight thermoelectric modules consisting of stacked NW network films that are connected electrically in series and thermally in parallel can be obtained. These observations hold promise for active cooling of electronic devices and waste energy harvesting using extremely light and flexible thermoelectric generators and could lead to advances in future spin caloritronic devices.

MATERIALS AND METHODS

Sample fabrication

The PC porous membranes with interconnected pores have been fabricated by exposing a 22-μm-thick PC film to a two-step irradiation process. The topology of the membranes was defined by exposing the film to a first irradiation step at two fixed angles of −25° and +25° with respect to the normal axis of the film plane. After rotating the PC film in the plane by 90°, the second irradiation step took place at the same fixed angular irradiation flux to finally form a 3D nanochannel network. The diameter of the latent tracks was enlarged by following a previously reported protocol to obtain membranes with distinct porosities and pores sizes (*37*). The PC membranes with average pore diameters of 80 and 105 nm display low volumetric porosity (3%) and large volumetric porosity (22%), respectively. Next, the PC templates were coated on one side using an e-beam evaporator with a metallic Cr/Au bilayer to serve as cathode during the electrochemical deposition. The thickness of the thin adhesion layer of Cr was 3 nm, while for a uniform and consistent nanopore coverage withstanding the electrodeposition process, the Au film thickness was set to 400 and 750 nm for the 80- and 105-nm-diameter porous membranes, respectively.

The multilayered NW networks have been grown at RT by electrodeposition into the 3D porous PC templates from a single sulfate bath using potentiostatic control and a pulsed electrodeposition technique (*38*). For these experiments, we used an Ag/AgCl reference electrode and a Pt counter electrode. To prepare the CoNi/Cu interconnected NW networks, the composition of the electrolyte was 2.3 M $NiSO_4 \cdot 6H_2O$ + 0.4 M $CoSO_4 \cdot 7H_2O$ + 15 mM $CuSO_4 \cdot 5H_2O$ + 0.5 M H_3BO_3, and the deposition potential was alternatively switched between −1 V to deposit equiatomic CoNi alloy layer (containing approximately 5% Cu impurity), and −0.4 V to deposit almost pure Cu layers (*39*). Following a procedure described elsewhere (*38*), the deposition rates of each metals were determined from the pore filling time. According to this calibration, the deposition time was adjusted

to 300 ms and 12 s for the CoNi and Cu layers, respectively, and the estimated average thickness of the bilayer was ~15 nm, with approximately the same thicknesses for the CoNi and Cu layers. The morphology of the nanostructured interconnected NW networks was characterized using a high-resolution field emission SEM JEOL 7600F equipped with an energy-dispersive x-ray analyzer. For the electron microscopy analysis, we removed the PC template by chemical dissolution using dichloromethane. For conducting magnetotransport measurements, the cathode was locally removed by plasma etching to create a two-probe design suitable for electric measurements, with the flow of current restricted along the NW segments, thus perpendicular to the plane of the layers.

Magnetothermoelectric measurements

The thermoelectric power was measured by attaching one end of the sample to the copper sample holder using silver paint and a resistive heater to the other end. The voltage leads were made of thin Chromel P wires, and the contribution of the leads to the measured thermoelectric power was subtracted out using the recommended values for the absolute thermopower of Chromel P. The temperature gradient was monitored with a small-diameter type E differential thermocouple. A typical temperature difference of 1 K was used in the measurements. The magneto-Seebeck measurements were made using low volumetric porosity PC membranes, with NWs partially filling the nanopores. A second setup was built to unambiguously highlight Peltier effects in NW networks grown in high volumetric porosity PC membranes with the nanopores completely filled with NWs to reduce the sample electrical resistance below 2 ohms and, consequently, the effects of Joule heating. In this case, two small Cernox thin film resistance sensors (<3 mg, 1 mm^2; Cernox 1010, Lake Shore Cryotronics Inc.) were attached at the junctions between the NW network and the metal electrodes. The temperature resolution of these highly sensitive thermometers is about 1 mK, which enables detection of Peltier effect–based heating or cooling while a DC electrical current is flowing through the junction between the NW network and the metal electrodes. All magnetotransport measurements were performed under vacuum with the magnetic field up to 1 T applied both in the plane and perpendicular to the plane of NW network films embedded in polymer membrane films. The temperature of the samples can be varied from 10 to 320 K.

SUPPLEMENTARY MATERIALS

Supplementary material for this article is available at http://advances.sciencemag.org/cgi/content/full/5/3/eaav2782/DC1

Section S1. Basic magnetic, magnetoresistance, and thermoelectric property characterization
Section S2. Estimation of the resistivity for the CoNi/Cu NW network
Section S3. Expression for the diffusion thermopower in the two-current model
Section S4. Relationship between the field-dependent thermopower and electrical resistance
Section S5. Data on magneto-Peltier
Section S6. Experimental measurement uncertainty evaluation
Fig. S1. Magnetic characterization curves.
Fig. S2. Gorter-Nordheim characteristics.
Fig. S3. Peltier temperature measurements at the Peltier junction B.
Fig. S4. Magneto-Joule and magneto-Peltier temperature measurements at the Peltier junction B.
References (*40*–*42*)

REFERENCES AND NOTES

1. J. He, T. M. Tritt, Advances in thermoelectric materials research: Looking back and moving forward. *Science* **357**, eaak9997 (2017).
2. G. E. W. Bauer, E. Saitoh, B. J. van Wees, Spin caloritronics. *Nat. Mater.* **11**, 391–399 (2012).
3. S. R. Boona, R. C. Myers, J. P. Heremans, Spin caloritronics. *Energy Environ. Sci.* **7**, 885–910 (2014).
4. K. Uchida, J. Xiao, H. Adachi, J. Ohe, S. Takahashi, J. Ieda, T. Ota, Y. Kajiwara, H. Umezawa, H. Kawai, G. E. W. Bauer, S. Maekawa, E. Saitoh, Spin Seebeck insulator. *Nat. Mater.* **9**, 894–897 (2010).
5. C. M. Jaworski, J. Yang, S. Mack, D. D. Awschalom, J. P. Heremans, R. C. Myers, Observation of the spin-Seebeck effect in a ferromagnetic semiconductor. *Nat. Mater.* **9**, 898–903 (2010).
6. A. Slachter, F. L. Bakker, J.-P. Adam, B. J. van Wees, Thermally driven spin injection from a ferromagnet into a non-magnetic metal. *Nat. Phys.* **6**, 879–882 (2010).
7. M. Hatami, G. E. W. Bauer, Q. Zhang, P. J. Kelly, Thermal spin-transfer torque in magnetoelectronic devices. *Phys. Rev. Lett.* **99**, 066603 (2007).
8. A. Pushp, T. Phung, C. Rettner, B. P. Hughes, S.-H. Yang, S. S. P. Parkin, Giant thermal spin-torque–assisted magnetic tunnel junction switching. *Proc. Natl. Acad. Sci. U.S.A.* **112**, 6585–6590 (2015).
9. M. J. Conover, M. B. Brodsky, J. E. Mattson, C. H. Sowers, S. D. Bader, Magnetothermopower of Fe / Cr superlattices. *J. Magn. Magn. Mater.* **102**, L5–L8 (1991).
10. L. Piraux, A. Fert, P. A. Schroeder, R. Loloee, P. Etienne, Large magnetothermoelectric power in Co/Cu, Fe/Cu and Fe/Cr multilayers. *J. Magn. Magn. Mater.* **110**, L247–L253 (1992).
11. J. Shi, S. S. P. Parkin, L. Xing, M. B. Salamon, Giant magnetoresistance and magnetothermopower in Co/Cu multilayers. *J. Magn. Magn. Mater.* **125**, L251–L256 (1993).
12. J. Shi, K. Pettit, E. Kita, S. S. P. Parkin, R. Nakatani, M. B. Salamon, Field-dependent thermoelectric power and thermal conductivity in multilayered and granular giant magnetoresistive systems. *Phys. Rev. B* **54**, 15273–15283 (1996).
13. E. Y. Tsymbal, D. G. Pettifor, H. Ehrenreich, F. Spaepen, *Perspectives of Giant Magnetoresistance* (Academic Press, 2001), vol. 56, pp. 113–237.
14. S. F. Lee, W. P. Pratt Jr., R. Loloee, P. A. Schroeder, J. Bass, "Field-dependent interface resistance" of Ag/Co multilayers. *Phys. Rev. B* **46**, 548–551 (1992).
15. J. Bass, CPP magnetoresistance of magnetic multilayers: A critical review. *J. Magn. Magn. Mater.* **408**, 244–320 (2016).
16. T. Farrell, D. Greig, The thermoelectric power of nickel and its alloys. *J. Phys. C Solid State Phys.* **3**, 138 (1970).
17. M. C. Cadeville, J. Roussel, Thermoelectric power and electronic structure of dilute alloys of nickel and cobalt with d transition elements. *J. Phys. F Metal Phys.* **1**, 686 (1971).
18. F. J. Blatt, P. A. Schroeder, C. L. Foiles, D. Greig, *Thermoelectric Power of Metals* (Springer, 1976).
19. S. J. Watzman, R. A. Duine, Y. Tserkovnyak, S. R. Boona, H. Jin, A. Prakash, Y. Zheng, J. P. Heremans, Magnon-drag thermopower and nernst coefficient in Fe, Co, and Ni. *Phys. Rev. B* **94**, 144407 (2016).
20. K. Vandaele, S. J. Watzman, B. Flebus, A. Prakash, Y. Zheng, S. R. Boona, J. P. Heremans, Thermal spin transport and energy conversion. *Mater. Today Phys.* **1**, 39–49 (2017).
21. L. Gravier, A. Fábián, A. Rudolf, A. Cachin, J.-E. Wegrowe, J.-P. Ansermet, Spin-dependent thermopower in Co/Cu multilayer nanowires. *J. Magn. Magn. Mater.* **271**, 153–158 (2004).
22. L. Gravier, S. Serrano-Guisan, F. Reuse, J.-P. Ansermet, Spin-dependent Peltier effect of perpendicular currents in multilayered nanowires. *Phys. Rev. B* **73**, 052410 (2006).
23. J. Flipse, F. L. Bakker, A. Slachter, F. K. Dejene, B. J. van Wees, Direct observation of the spin-dependent peltier effect. *Nat. Nanotechnol.* **7**, 166–168 (2012).
24. T. Böhnert, A. C. Niemann, A.-K. Michel, S. Bäßler, J. Gooth, B. G. Tóth, K. Neuróhr, L. Péter, I. Bakonyi, V. Vega, V. M. Prida, K. Nielsch, Magnetothermopower and magnetoresistance of single Co-Ni/Cu multilayered nanowires. *Phys. Rev. B* **90**, 165416 (2014).
25. N. Liebing, S. Serrano-Guisan, K. Rott, G. Reiss, J. Langer, B. Ocker, H. W. Schumacher, Tunneling magnetothermopower in magnetic tunnel junction nanopillars. *Phys. Rev. Lett.* **107**, 177201 (2011).
26. M. Walter, J. Walowski, V. Zbarsky, M. Münzenberg, M. Schäfers, D. Ebke, G. Reiss, A. Thomas, P. Peretzki, M. Seibt, J. S. Moodera, M. Czerner, M. Bachmann, C. Heiliger, Seebeck effect in magnetic tunnel junctions. *Nat. Mater.* **10**, 742–746 (2011).
27. F. K. Dejene, J. Flipse, B. J. van Wees, Spin-dependent Seebeck coefficients of $Ni_{80}Fe_{20}$ and Co in nanopillar spin valves. *Phys. Rev. B* **86**, 024436 (2012).
28. J. Shan, F. K. Dejene, J. C. Leutenantsmeyer, J. Flipse, M. Münzenberg, B. J. van Wees, Comparison of the magneto-Peltier and magneto-Seebeck effects in magnetic tunnel junctions. *Phys. Rev. B* **92**, 020414 (2015).
29. T. da Câmara Santa Clara Gomes, J. De La Torre Medina, Y. G. Velázquez-Galván, J. M. Martínez-Huerta, A. Encinas, L. Piraux, Interplay between the magnetic and magneto-transport properties of 3d interconnected nanowire networks. *J. Appl. Phys.* **120**, 043904 (2016).
30. T. da Câmara Santa Clara Gomes, J. De La Torre Medina, M. Lemaitre, L. Piraux, Magnetic and magnetoresistive properties of 3D interconnected nico nanowire networks. *Nano. Res. Lett.* **11**, 466 (2016).
31. E. Araujo, A. Encinas, Y. Velázquez-Galván, J. M. Martínez-Huerta, G. Hamoir, E. Ferain, L. Piraux, Artificially modified magnetic anisotropy in interconnected nanowire networks. *Nanoscale* **7**, 1485–1490 (2015).
32. L. Piraux, J. M. George, J. F. Despres, C. Leroy, E. Ferain, R. Legras, K. Ounadjela, A. Fert, Giant magnetoresistance in magnetic multilayered nanowires. *Appl. Phys. Lett.* **65**, 2484–2486 (1994).

33. O. Yamashita, S. Tomiyoshi, K. Makita, Bismuth telluride compounds with high thermoelectric figures of merit. *J. Appl. Phys.* **93**, 368–374 (2002).
34. O. Bubnova, Z. U. Khan, A. Malti, S. Braun, M. Fahlman, M. Berggren, X. Crispin, Optimization of the thermoelectric figure of merit in the conducting polymer poly(3,4-ethylenedioxythiophene). *Nat. Mater.* **10**, 429–433 (2011).
35. M. N. Ou, T. J. Yang, S. R. Harutyunyan, Y. Y. Chen, C. D. Chen, S. J. Lai, Electrical and thermal transport in single nickel nanowire. *Appl. Phys. Lett.* **92**, 063101 (2008).
36. M. Zebarjadi, Electronic cooling using thermoelectric devices. *Appl. Phys. Lett.* **106**, 203506 (2015).
37. E. Ferain, R. Legras, Track-etch templates designed for micro- and nanofabrication. *Nucl. Instrum. Methods Phys. Res. B* **208**, 115–122 (2003).
38. A. Fert, L. Piraux, Magnetic nanowires. *J. Magn. Magn. Mater.* **200**, 338–358 (1999).
39. X.-T. Tang, G.-C. Wang, M. Shima, Layer thickness dependence of CPP giant magnetoresistance in individual CoNi/Cu multilayer nanowires grown by electrodeposition. *Phys. Rev. B* **75**, 134404 (2007).
40. J. De La Torre Medina, M. Darques, T. Blon, L. Piraux, A. Encinas, Effects of layering on the magnetostatic interactions in microstructures of Co_xCu_{1-x}/Cu nanowires. *Phys. Rev. B* **77**, 014417 (2008).
41. B. G. Tóth, L. Péter, Á. Révész, J. Pádár, I. Bakonyi, Temperature dependence of the electrical resistivity and the anisotropic magnetoresistance (AMR) of electrodeposited Ni-Co alloys. *Eur. Phys. J. B* **75**, 167–177 (2010).
42. T. Valet, A. Fert, Theory of the perpendicular magnetoresistance in magnetic multilayers. *Phys. Rev. B* **48**, 7099–7113 (1993).

Acknowledgments: We thank E. Ferain and the it4ip Company for supplying PC membranes. **Funding:** Financial support was provided by Wallonia/Brussels Community (ARC 13/18-052) and the Belgian Fund for Scientific Research (FNRS). T.d.C.S.C.G. and F.A.A. are research fellows of the FNRS. **Author contributions:** L.P. conceived and designed the two Seebeck and Peltier sample holders and wrote the manuscript. F.A.A. conceived, designed, and developed the experimental measurement setups for magnetotransport, Seebeck, and Peltier measurements. T.d.C.S.C.G. fabricated the samples and performed characterization experiments and the magnetotransport, Seebeck, and magneto-Seebeck measurements. F.A.A. performed the Peltier and the magneto-Peltier measurements. All authors analyzed the results and commented on the manuscript. **Competing interests:** The authors declare that they have no competing interests. **Data and materials availability:** All data needed to evaluate the conclusions in the paper are present in the paper and/or the Supplementary Materials. Additional data related to this paper may be requested from the authors.

Submitted 31 August 2018
Accepted 11 January 2019
Published 1 March 2019
10.1126/sciadv.aav2782

Citation: T. da Câmara Santa Clara Gomes, F. Abreu Araujo, L. Piraux, Making flexible spin caloritronic devices with interconnected nanowire networks. *Sci. Adv.* **5**, eaav2782 (2019).